Probing the Structural Features and the Micro-heterogeneity of Various Deep Eutectic Solvents and their Water Dilutions by the Photophysical Behaviour of Two Fluorophores

Matteo Tiecco,[a] Irene Di Guida,[a] Pier Luigi Gentili,[a] Raimondo Germani,[a] Carmela Bonaccorso,[b] Alessio Cesaretti[a,*]

[a] Dipartimento di Chimica, Biologia e Biotecnologia and Centro di Eccellenza sui Materiali Innovativi Nanostrutturati (CEMIN), Università degli Studi di Perugia, via Elce di Sotto 8, 06123 Perugia, Italy.

[b] Dipartimento di Scienze Chimiche, Università degli Studi di Catania, viale Andrea Doria 6, 95125 Catania, Italy.

* Corresponding Author. ORCID: 0000-0001-5814-8524; e-mail address: alex.cesaretti14@gmail.com

ABSTRACT

The structural features of a series of diverse Deep Eutectic Solvents (DESs) have been investigated and characterized by means of two fluorescent probes. The spectral and photophysical properties of the latter are strictly dependent on the experienced environment, so that they can provide insights into the polarity, viscosity, hydrogen-bond network, and micro-heterogeneity of the various DESs.

In fact, the investigated DESs exhibit a variety of properties with regards to their hydrophilicity, acidity, and hydrogen-bond ability, and these details were deeply probed by the two fluorescent molecules. The effect of the addition of water, which is a key strategy for tuning the properties of these structured systems, was also tested. In particular, the excited state dynamics of the probes, measured by femtosecond-resolved transient absorption, proved instrumental in understanding the changes in the structural properties of the DESs, namely reduced viscosity and enhanced heterogeneity, as the water percentage increases. Differences between the various DESs in terms of both local microheterogeneity and bulk viscosity also emerged from the peculiar multi-exponential solvation dynamics undergone by the excited states of the probes.

The appraisal of a different local heterogeneity, depending on either the nature of the DES or the amount of added water, was also supported by the maximum entropy method (MEM) applied to the fluorescence decay kinetics, which gave clear indications about the different micro-heterogeneity of the DES systems.

KEYWORDS

Microheterogeneity; Structural Water; Fluorescent Probe; Ultrafast Spectroscopy; Solvation Dynamics; Maximum Entropy Method.

INTRODUCTION

Deep Eutectic Solvents (DESs) are a novel class of organic solvents that are finding fruitful applications in many topics in the recent years thanks to their green and catalytic properties [1–4]. These liquids are formed by simply mixing and heating two compounds (often solids) that have hydrogen bond donor (HBD) and hydrogen bond acceptor (HBA) properties, respectively; the mixture of weak interactions occurring between the two different species and between the molecules of the same species, determine a non-ideal behavior of their melting points because of the difficult crystal lattice formation [5,6]. DESs can be divided in different sub-classes depending on the molecules forming them but they are usually formed by an "*onium*" salt with an HBD molecule, that decrease the strength of interaction of the two ions of the salt thanks to H-bonds [3]. However, in literature many novel classes of DESs also formed by neutral or zwitterionic species are reported; a wide number of molecules can be used as HBD or HBA to form DESs, leading to a high number of possible novel mixtures with a wide range of different characteristics [7,8].

DESs show two main relevant features: they are environmentally friendly and they can show catalytic activity [4,9,10].

DESs possess green properties for different reasons: they have low or absent vapour pressure (therefore they also permit to develop "out of the hood" procedures, determining also a reduction in the costs of the facilities for the procedures); they are non-toxic; they can be formed by natural molecules (NADESs, Natural Deep Eutectic Solvents), with increased bioavailability and biodegradability; they can be easily recycled in subsequent procedures and so on [11–19]. For these reasons, DESs, born as a side-class of ionic liquids, are increasing their relevance over the other liquids in the green chemistry framework in the recent years [20].

The catalytic properties of the DESs are principally determined by the characteristics of their components, but also other properties of the liquids must be considered in order to evaluate the "activity" of these solvents [21–25]. In literature, many cases of acidic catalysis performed by these mixtures are reported, but also other catalytic properties are gaining relevance such as reducing capabilities and also organocatalytic behaviour in asymmetric synthesis (with CDESs: chiral-DESs). In the particular topic of asymmetric catalysis, the properties of the novel liquids revealed to be determined by the intimacy of HBD-HBA couple and therefore on the availability of the organocatalyst in terms of association constant between the two components [26,27]. On the other hand, more structured systems led to higher enantiomeric excesses in the probe reactions thanks to the steric hindrance of one of the two faces of the adducts. This effect was also observed with other acid liquids where the properties were dependent on the pKa of the components but with different entities compared to the properties of the pure HBD, suggesting a different availability of the molecule to act in its own way [28]. The same effect exerted by the intimacy of the couple was observed in studies regarding the CO_2 capture driven by these innovative solvents [29].

A peculiar and relevant effect was observed in the studies involving DESs/water mixtures [30–32]. In this case, as water is the most relevant H-bonds capable molecule, the interactions with the HBD and HBA of the DESs lead to: "structural" water at concentration lower than about 15% w/w; persistence of HBD-HBA interactions of the DESs until about 50-60% w/w of water (therefore HBD-HBA clusters formation); disruption of the DESs structures at concentrations of water over 60% w/w. The properties of the liquids (such as viscosity, conductivity, density and so on) can be also tailored by specific amounts of added water in DESs mixtures; i.e., their viscosity can drastically decrease even with small amounts of added water. Other relevant DESs in this topic are the hydrophobic ones: mixtures that are formed by H-bonds but that can be separated from water only by the use of hydrophobic HBD components [33–35].

Therefore, the complexity of these systems needs a deep understanding of their structural features in order to comprehend and therefore control properly their properties.

Many papers are reported in literature with a microscopic study approach to novel liquids, with different techniques and with different aims [6,36–39]. In many of these papers, the inhomogeneity of the microscopic structural features is underlined, that is also, as mentioned before, the reason for the liquid formation. Fluorescent probe studies were also used in these approaches in order to investigate the structural features of these systems [40–45]. In particular, a

great deal of effort has recently been put in trying and understanding the difference between spatial and temporal heterogeneity in various DESs. Time-resolved spectroscopic techniques evidenced micro-heterogeneity in the relaxation dynamics of the fluorescent probes, in terms of diffusion and rotation times of the solute. These studies revealed strong dynamic heterogeneity originated from modification of the H-bond network by virtue of H-bond reorientations and collective H-bond relaxations, while signatures of either mild or high spatial micro-heterogeneity were collected depending on the investigated DESs. Other studies have instead focused on the complete solvation dynamics of the solvent shell around the probes, investigated by both fluorescence and FTIR spectroscopy and supported by molecular dynamics simulations [45–49]. Solvation times ranging from a sub-picosecond time-scale to hundreds of picoseconds were recorded and the slow components of the solvent response function was found to well correlate with the macroscopic viscosity of different DESs.

In order to shed light on the structural features of a set of differently structured DESs, a spectroscopic femtosecond-resolved study is proposed in this work with the use of suitable fluorescence probes, whose photophysical properties and excited state dynamics have already been deeply investigated in our laboratory [50–54]. Specifically, an N-methylpyridinium iodide (2-4-(diphenylamino)phenyl-ethenyl-1-methylpyridinium iodide, **PyI**) was chosen as a polarity and viscosity probe, while a phenanthroline derivative (4,4'-((1E,1'E)-(1,10-phenanthroline-2,9-diyl)bis(ethene-2,1-diyl))bis(3-methoxy-N,N-dimethylaniline, **X5**), showing fluorosolvatochromism and bearing protonation sites, was used as polarity and H-bond probe.

The diverse DESs analysed in this work have different properties as they are hydrophobic or hydrophilic, they have different acidic properties (from neutral, to weak, to strong acids forming them), and they were analysed also in their mixtures with water. The structures of the molecules forming the liquids, as well as the ones of the fluorescent probes **PyI** and **X5**, are reported in Scheme 1.

From these studies, the existence of differences between the various DESs stands out in terms of polarity, viscosity, and hydrogen-bond ability. Further, an increased spatial micro-heterogeneity was revealed in all the DESs as a function of added water. Finally, in the special case of the *p*-toluenesulfonic acid-based DES (**pTSA/TBnAMSO**), a different level of structural organization was seized between the higher disorder observed in the cybotactic region of the probe (reduced local viscosity) and the greater organization detected in its long-range solvation shell (increased bulk viscosity).

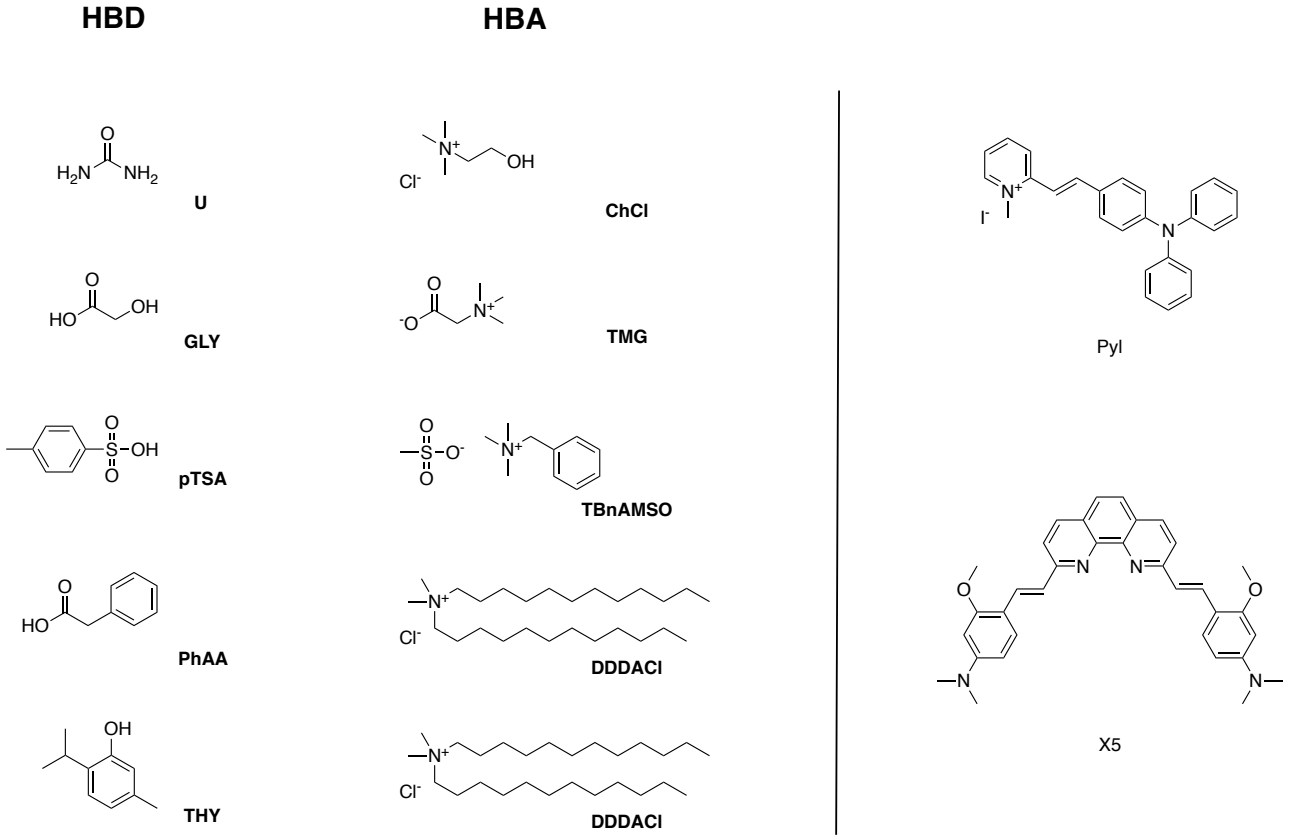

Scheme 1: Deep Eutectic Solvents analyzed (left): **U** (urea) / **ChCl** (choline chloride) 2/1 molar ratio; **GLY** (glycolic acid) / **TMG** (trimethylglycine) 2/1 molar ratio; **pTSA•H_2O** (*p*-toluenesulfonic acid•H_2O) / **TBnAMSO** (trimethylbenzylammonium methanesulfonate) 1/1 molar ratio; **PhAA** (phenylacetic acid) / **DDDACl** (N,N,N,N-dimethyldidodecylammonium chloride) 2/1 molar ratio; **THY** (thymol) / **DDDACl** (N,N,N,N-dimethyldidodecylammonium chloride) 2/1 molar ratio. Fluorescent probes (right): **Pyl** (2-4-(diphenylamino)phenyl-ethenyl-1-methylpyridinium iodide); **X5** 4,4'-((1E,1'E)-(1,10-phenanthroline-2,9-diyl)bis(ethene-2,1-diyl))bis(3-methoxy-N,N-dimethylaniline.

EXPERIMENTAL

MATERIALS

The investigated fluorescent probes (shown in Scheme 1) were synthesized as described in reference [51] for **Pyl** and in reference [50] for **X5**.

DESs PREPARATION

Urea, choline chloride, glycolic acid, trimethylglycine, *p*-toluenesulfonic acid monohydrate, phenylacetic acid were purchased from Sigma-Aldrich, Merck and Alfa Aesar (purities >98%) and were used without further purifications. N,N,N,N-dimethyldidodecylammonium chloride and trimethylbenzylammonium methanesulfonate were synthesised following the procedures reported in our previous papers [34,55]. Deep Eutectic Solvents were prepared following the procedures reported in our previous works: HBD and HBA components were mixed in a screw-

capped vial. The solid mixture was magnetically stirred and heated at 60°C for 20–60 min until a clear colourless liquid was obtained. The water content of the pure DESs and their water dilution were measured via Karl-Fischer titration with Metrohm 684 KF Coulometer; the water solutions of the DESs were prepared by adding the proper amount of water to the DESs samples and stirring them at room temperature overnight. The liquids showed starting water amounts spanning from 1% to 2% w/w except for **pTSA/TBnAMSO** system that showed higher values (about 4% w/w) due to hydration water molecule of pTSA.

VISCOSITY MEASUREMENTS

The viscosity of the eutectic mixtures was measured using a Fungilab Expert L viscometer, fitted with a thermostatic jacket and a temperature probe. The viscometer jacket was connected to an external thermostated bath (25.0 $\pm$ 0.1°C). The viscosity measurements were obtained using a spindle attachment.

STEADY-STATE ABSORPTION AND EMISSION SPECTROSCOPIES

Steady-state UV-Visible absorption spectra have been recorded by using a PerkinElmer Lambda 800 spectrophotometer for air-equilibrated solutions. Luminescence spectra have been collected by a Horiba FluoroMax-4 spectrofluorimeter of HORIBA Scientific operated by FluorEssence. The latter gives back fluorescence emission spectra considering corrections for both the monochromator response and the detector sensitivity. Fluorescence quantum yields (experimental error of ca. 5%) have been determined from the emission spectra of samples whose absorbance at the excitation wavelength was lower than 0.1. The absorbance was maintained smaller than 0.1 to have a linear relationship between the absorbance and the emission intensity and avoid self-absorption effects. Tetracene (ϕ_F =0.16 in air-equilibrated cyclohexane) [56] has been used as the fluorometric standard for the determination of the fluorescence quantum yields. The quantum yields of the two fluorophores in the different DESs have been estimated using equation (1):

$$\Phi_X = \Phi_{st}\left(\frac{I_X}{I_{st}}\right)\left(\frac{A_{st}}{A_X}\right)\left(\frac{n_X^2}{n_S^2}\right) \quad (1)$$

In equation (1), I_X, A_X, and n_X stand for the total emission intensity, absorbance at the excitation wavelength, and refractive index of the DES with the fluorophore, respectively, whereas I_{st}, A_{st}, and n_{st} are the same parameters relative to the tetracene solution. The refractive index n_X of the DESs have been determined by using an Abbe refractometer (Officine Galileo).

FLUORESCENCE LIFETIMES

The fluorescence lifetimes (τ_F) have been measured by using a spectrofluorometer (Edinburgh Instrument 199S) based on the single photon counting technique, equipped for the systems under investigation with a LED source centred at 461 nm, using an interference filter centred at 460 nm in the excitation line and a long-pass filter in emission at 488 nm. A Hamamatsu R7400U-03 photomultiplier tube has been used as detector. The resolution time of the experimental set-up is about 200 ps when the 461 nm LED source is used. The luminesce decay kinetics have been analysed through the Maximum Entropy Method (MEM) using the MEMEXP software [57,58]. In the Maximum Entropy Method, the experimental decay $I(t)$ is fitted by the following function:

$$I(t) = D_0 \int_{-\infty}^{+\infty} d\,log\,\tau\,[f(log\,\tau)] * \int_{-t_0}^{min(t,t_f)} dt' R(t') e^{-(t_i - t')/\tau} \quad (2)$$

where *f(log τ)* is the decay time distribution that corresponds to decay kinetics. The instrument response function $R(t')$ is peaked at zero time and is appreciable only in the [-t_0, t_f] interval. The rise kinetics and the polynomial term accounting for the baseline are not considered in our model since our data show neither increase nor scattering. The fit procedure entails the maximization of the function Q defined in equation (3):

$$Q = S - \lambda C - \alpha M \quad (3)$$

In (3), S is entropy, defined as $S(\vec{f}, \vec{F}) = \sum_{i=1}^{N} [f_i - F_i - f_i\, ln(f_i/F_i)]$, where $\vec{F}$ is the uniform MEM prior distribution used to incorporate prior knowledge into the solution. C is the Poisson deviance. *M* is a normalization factor; *N* is the total number of lifetimes used in the fitting procedure; λ and α are Lagrange multipliers.

ULTRAFAST SPECTROSCOPY

The experimental setups for femtosecond transient absorption measurements have been widely described elsewhere [59–61]. In particular, the 400 nm excitation pulses of ca. 40 fs are generated by an amplified Ti:Sapphire laser system (Spectra Physics). The transient absorption set up (Helios, Ultrafast Systems) is characterized by temporal resolution of ca. 150 fs and spectral resolution of 1.5 nm. Probe pulses are produced in the 450–800 nm range by passing a small portion of 800 nm light through an optical delay line (with a time window of 3200 ps) and focusing it into a 2 mm thick Sapphire window to generate a white–light continuum. Ultrafast spectroscopic data were fitted by Global and Target Analysis using Surface Explorer and Glotaran softwares [62,63].

RESULTS AND DISCUSSION

Spectral and photophysical properties of the two fluorophores in DESs

The two fluorophores were dissolved separately into the different DESs, and their photophysical properties were determined by recording their steady-state and time-resolved absorption and emission spectra. Both fluorophores are sensitive to the polarity of the medium: **PyI** features negative solvatochromism, that is its absorption spectrum shifts toward shorter wavelengths with increasing polarity [51]; while **X5** exhibits positive fluorosolvatochromism, with its emission spectrum shifting to longer wavelengths when the polarity of the medium increases [50]. Moreover, the excited state deactivation of **PyI** is characterized by the formation of a twisted intramolecular charge transfer state (TICT) and it is thus ruled by viscosity [53]. On the other hand, **X5** features an acidic centre on the central phenanthroline nitrogens with a pKa of 5.74, and its spectral properties are thus sensitive to the acidity of the environment [52] and H-bonding ability of the HBD component forming the DES.

As far as **PyI** is concerned, its absorption spectrum provides clear evidence of the different polarity established by the various DESs. As a rule, the absorption spectrum of **PyI** dissolved in DES exhibits a maximum in a spectral range typical of polar solvents (MeOH and W/EtOH mixtures) [51] proving the high polarity of the investigated systems. In particular, **PhAA/DDDACl** turns out to be the most polar medium, with the **PyI** absorption spectrum peaking at 440 nm (see Figure 1), close to the maximum recorded for the same molecule in a W/EtOH 95:5 (v/v) mixture. Then, a slightly reduced polarity is found in **GLY/TMG** and **U/ChCl** (λ_{abs} = 444 nm), followed by **pTSA/TBnAMSO** (λ_{abs} = 449 nm). Finally, the least polar among the studied DESs is **THY/DDDACl**, where **PyI** absorption peaks at 453 nm, resembling the position found in MeOH.

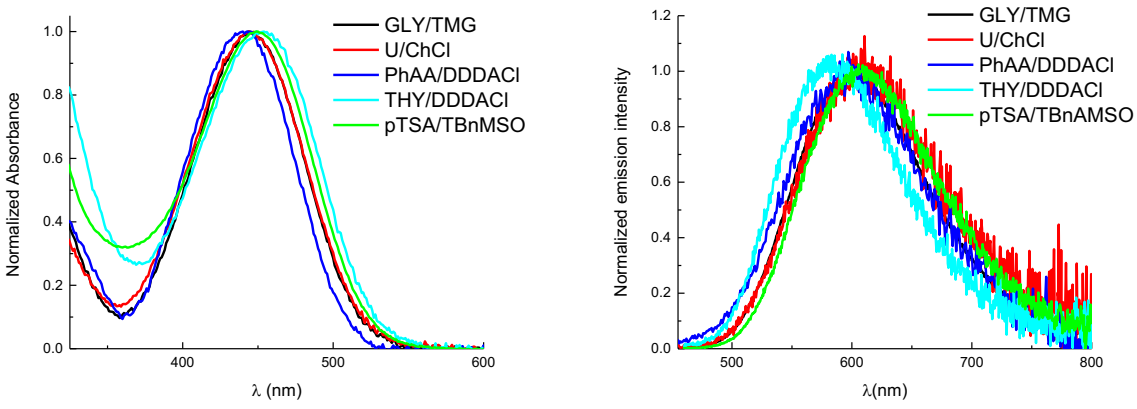

Figure 1. Normalized absorption (left) and emission (right) spectra of **PyI** in the different DESs.

Conversely, the fluorescence spectrum can provide information on the local viscosity and micro-heterogeneity of the environment. In fact, time-resolved fluorescence experiments previously performed on **PyI** in different solvents have demonstrated that its emission comes from both a locally excited state (LE) and a TICT state. Typically, the steady state fluorescence is the one coming from the relaxed TICT state and it is centred between 640 and 710 nm, depending on the solvent. However, the contribution from unrelaxed conformations emerges when viscosity is increased, thus impairing large amplitude motions and full relaxation in the excited state. This is the case of **PyI** in DES, where its fluorescence peaks between 584 and 608 nm (see Figure 1), revealing an incomplete relaxation. Differences can again be spotted among the various DESs and the reasonable deductions that can be made well correlate with the direct measurements of their bulk viscosities at 25°C: **THY/DDDACl** shows a high viscosity (λ_{em} = 584 nm; η = 809.04 cP); followed by **GLY/TMG** (λ_{em} = 599 nm; η = 678.83 cP); while a reduced viscosity is peculiar to **U/ChCl** (λ_{em} = 607 nm; η = 403.2 cP). Exceptions to this trend are represented by **PhAA/DDDACl** and **pTSA/TBnAMSO**. The former exhibits the lowest bulk viscosity (η = 376.22 cP), but a lower extent of excited state relaxation, as revealed by an emission band peaking at 596 nm. This finding could be rationalized taking into account the hydrophobic nature of this DES: in fact, some water is always absorbed by pure DESs; however, being both components in **PhAA/DDDACl** hydrophobic, its intrinsic water content is expected not to affect the HBA-HBD network, but instead to be present as structural water about the DES pairs. This water molecules could indeed be responsible for the low bulk viscosity measured for **PhAA/DDDACl**, but **PyI** is likely to be less exposed to water molecules and instead be intimately localized within the hydrophobic domain of the system where it undergoes a reduced relaxation, as reflected by its blue-shifted fluorescence band position. On the other hand, **PyI** emission maximum in **pTSA/TBnAMSO** (λ_{em} = 608 nm) would suggest a considerable degree of excited state relaxation, although a remarkably high viscosity was measured for this DES (η = 1426.92 cP). This peculiar behaviour will be later explained thanks to the results of the time-resolved excited state absorption measurements.

Straightforward information cannot instead be deduced from the fluorescence quantum yields, as it is affected by polarity and viscosity in a combined manner.

Conversely, other informative details emerge from the excited state lifetimes, which were estimated by the Maximum Entropy Method (MEM) applied to the kinetics recorded with the TC-SPC technique. This analytical tool is extremely powerful, as it has also been demonstrated in previous works [64–70]. The output of the fitting procedure explained in the Experimental Section

is a lifetime distribution wherein each lifetime, τ_i, has its weight, w_i, which is a number included between 0 and 1 (it becomes a percent weight, $\%w_i$, if multiplied by 100). The lifetime distribution gives information about the sample micro-heterogeneity, which might depend on the number of emitting species conformers and/or the number of different micro-environments that surround the luminophores. The lifetime distribution is usually described quantitatively by two parameters. The first one is the weighted average lifetime $\bar{\tau}_{w.a.}$ (equation (4)):

$$\bar{\tau}_{w.a.} = \sum_{i=1}^{N} w_i \tau_i \quad (4)$$

wherein N is the total number of exponential functions used in the fitting procedure.

The second one is the Fuzzy Entropy H (equation (5)):

$$H = -\frac{1}{log(N)} \sum_{i=1}^{N} (w_i log(w_i)) \quad (5)$$

H varies between 0 and 1 and gauges the micro-heterogeneity of the sample: the greater the Fuzzy Entropy, the broader the lifetime distribution, the higher the micro-heterogeneity.

The luminescence decay kinetics of **PyI** in the different DESs and the outputs of the fitting procedure carried out by MEM are shown in Figures S1-S5 of the SI. The $\bar{\tau}_{w.a.}$ and H values are listed in Table 1. The longest $\bar{\tau}_{w.a.}$ is observed in **THY/DDDACl**, being the most viscous DES, aside from the exceptional case of **pTSA/TBnAMSO**, whereas the shortest one is in **U/ChCl**. The largest H value is in **U/ChCl**, whereas the smallest one is in **THY/DDDACl**. The results concerning **pTSA/TBnAMSO** are again peculiar, in that it exhibits a long $\bar{\tau}_{w.a.}$, which well agrees with the great viscosity measured, but a large value of *H*, which would suggest a high microheterogeneity.

Table 1. Photophysical properties of **PyI** in the DESs

DES	λ_{abs}(nm)	λ_{em}(nm)	$\Delta\bar{\nu}$ (cm^{-1})	Φ_F	$\bar{\tau}_{w.a.}$(ns)*	H**
GLY/TMG	444	599	5830	0.21	1.67	0.634
U/ChCl	444	607	6050	0.11	1.32	0.666
PhAA/DDDACl	440	596	5950	0.11	1.61	0.626
THY/DDDACl	453	584	4950	0.14	2.24	0.556
pTSA/TBnAMSO	449	608	5820	0.35	2.05	0.640

*$\bar{\tau}_{w.a.}$ is the weighted average lifetime estimated by the Maximum Entropy Method

**H is the Fuzzy Entropy estimated by the Maximum Entropy Method

As for the other fluorophore **X5**, a clear difference emerges between DESs containing an acidic carboxylic group and those lacking it. The former, i.e., **GLY/TMG** and **PhAA/DDDACl**, imply the protonation of the phenanthroline nitrogen, resulting in significantly red-shifted absorption and emission spectra with respect to the ones recorded in **U/ChCl** and **Thy/DDDACl** (see Figure 2).

Moreover, the protonated **X5** has a shorter weighted average lifetime with respect to its unprotonated form (see Table 2 and Figures S6-S9 of the SI). As mentioned before, deprotonated **X5** fluorescence is sensitive to polarity and its position tells that **U/ChCl** provides a more polar environment than **THY/DDDACl**, confirming what has been probed by **PyI**. In fact, a higher polarity allows a greater stabilization for the charge-transfer excited state and thus a red-shifted emission. **X5** exhibits a fluorescence centred at 559 nm in **U/ChCl**, similar to the one recorded in the most polar solvents where the compound has previously been dissolved (EtOH or MeCN) [52]; whereas, in **THY/DDDACl**, **X5** fluorescence peaks at about 530 nm, resembling its emission in intermediate polarity solvents (*i.e.*, $CHCl_3$) [52].

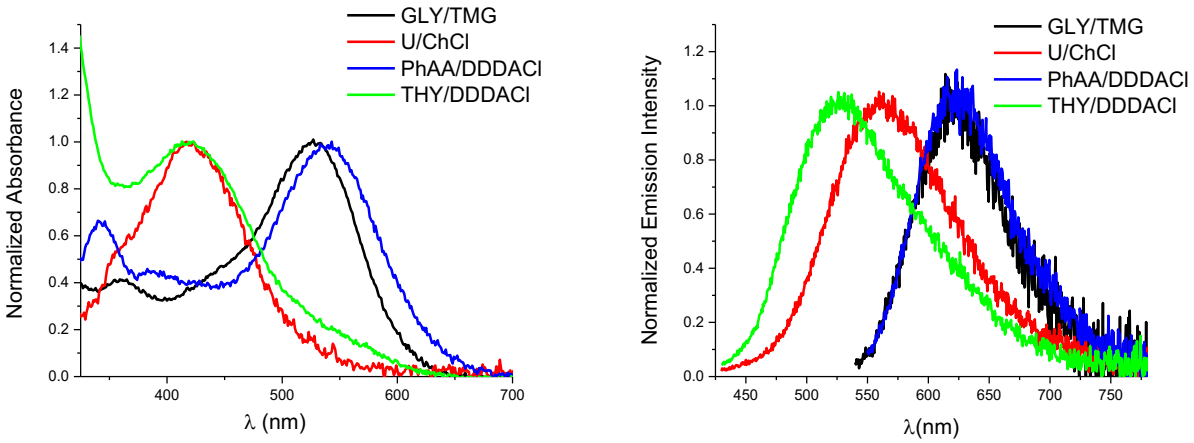

Figure 2. Normalized absorption (left) and emission (right) spectra of **X5** in the different DESs.

Differently from **PyI**, **X5** excited state is not influenced by viscosity; its dynamics is instead dependent on the proticity of the medium where the molecule is dissolved. **X5** forms intramolecular N···H interactions which planarize its conformation favouring more rigid structures which undergo radiative deactivation pathways. However, when solvent molecules can form intermolecular hydrogen bonds with **X5**, the latter moves from planarity and a certain conformational disorder is introduced, also implying a decrease in the fluorescence quantum yield and lifetime. This is also the case with the investigated DESs, both the fluorescence efficiency, the excited state lifetime, and the Fuzzy Entropy provide evidence of the disorder degree reached in the various DESs (see the data in Table 2). In particular, the highest emission, longest lifetime and lowest H values are peculiar to **U/ChCl**, implying a reduced ability to form hydrogen bonds with **X5**; while **DDDACl**-containing DESs feature a lower ϕ_F and the greatest H values, revealing strong intermolecular interactions with the probe and a broader conformational distribution.

Table 2. Photophysical properties of **X5** in DES

DES	λ_{abs}(nm)	λ_{em}(nm)	$\Delta\bar{\nu}$ (cm^{-1})	Φ_F	$\bar{\tau}_{w.a.}$(ns)*	H**
GLY/TMG	529	620	2770	0.01	0.67	0.729
U/ChCl	424	559	5700	0.17	1.43	0.673
PhAA/DDDACl	540	625	2540	0.04	0.72	0.791
THY/DDDACl	421	529	4850	0.04	1.27	0.834

*$\bar{\tau}_{w.a.}$ is the weighted average lifetime estimated by the Maximum Entropy Method
**H is the Fuzzy Entropy estimated by the Maximum Entropy Method

Water dilutions of DESs

The addition of water to the DESs was structurally investigated in order to understand the role of H-bonds in the water dilutions. Moreover, macroscopic properties of the liquids, such as the viscosity, are heavily impacted even by small amounts of added H_2O [31,32,71]. The first steps of these measures were performed with amounts of water lower than 20% w/w. As emerged from previous studies, also hydrophobic or water-separable DESs can in fact absorb small amounts of water until values of about 15-20% w/w, with entities depending on the molecular structures of the components [34]. Therefore, in this study also nominally hydrophobic DESs such as **PhAA/DDDACl** were analyzed with this approach, as these amounts of water, called structural water [31,32], can have a strong effect on the viscosity of the liquids. The effect of the introduction of water in DESs was studied resorting to the viscosity-dependent **PyI** probe, whose photophysical properties are reported in Tables 3, S1 and S2 and Figures S10-S12 as a function of added water percentages. When dealing with hydrophilic mixtures, namely **GLY/TMG** and **pTSA/TBnAMSO**, the polarity of the environment is not altered by the introduction of water, as evidenced by the invariant absorption position; conversely, both the fluorescence maximum and quantum yield are significantly changed as a consequence of a net reduction in viscosity. This is especially the case of **GLY/TMG**, where the quantum yield drops by over one order of magnitude with increasing water percentages, following a trend that parallels the viscosity values, which were independently measured (Figure 3). An analogous trend was obtained for **pTSA/TBnAMSO**, but the effect in this case is less pronounced. This could reveal a reduced ability for water molecules to disrupt the HBD-HBA interactions responsible for the high bulk viscosity especially peculiar to this structured DESs.

As for the hydrophobic **PhAA/DDDACl** mixture, an even weaker effect was observed for the reduction of **PyI** fluorescence quantum yield: in this case the hydrophobicity of the liquid itself could play a relevant part as water could weakly interact with HBD and HBA molecules, which are

both scarcely hydrophilic, and instead it could arrange to form free water domains. Interestingly enough, **PyI** absorption and emission maximum positions are affected in a peculiar way in this hydrophobic DES: the absorption spectrum is shifted toward higher energies, while the fluorescence spectrum is slightly altered by the increasing water content. The latter finding suggests that **PyI** prefers the hydrophobic domains provided by the DES, so that water molecules do not influence its excited state relaxation and fluorescence emission to a great extent. On the other hand, the blue-shift of the absorption, to even higher energies relatively to **PyI** absorption spectrum in pure water, reveals the extreme polarity of the **PhAA/DDDACl** DES and again its ability to subtract the dye from the aqueous domains.

Table 3. Photophysical properties of **PyI** in **GLY/TMG** with different amounts of water.

% water	λ_{abs}(nm)	λ_{em}(nm)	$\Delta\bar{\nu}$ (cm^{-1})	Φ_F
2.85	444	599	5828	0.21
7.71	444	618	6341	0.06
12.58	444	625	6523	0.04
17.32	444	634	6750	0.02
22.37	444	637	6824	0.01

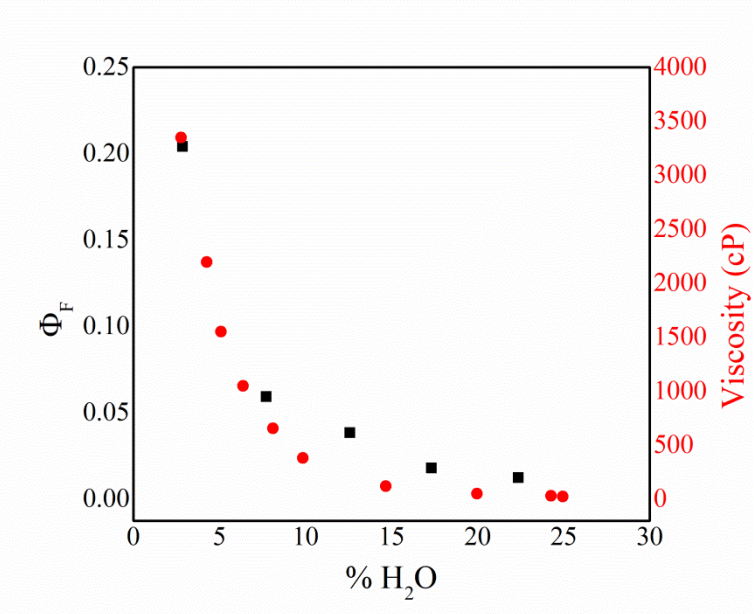

Figure 3. Trends of the fluorescence quantum yield of **PyI** in **GLY/TMG** and viscosity of the DES as a function of different amounts of water.

Also, the lifetime distributions of **PyI** are significantly affected by water additions. Figures 4A, 4B, and 4C show the lifetime distributions in **GLY/TMG**, **pTSA/TBnAMSO**, and **PhAA/DDDACl,**

respectively, after additions of different amounts of water. In all the three cases, $\bar{\tau}_{w.a.}$ shortens, while H rises by increasing water percentage. After the addition of a 20% of water in **GLY/TMG** and **pTSA/TBnAMSO**, $\bar{\tau}_{w.a.}$ decreases by 80% and 84%, respectively. After the addition of a 15% of water in **PhAA/DDDACl,** $\bar{\tau}_{w.a.}$ lowers by 65%. The water addition determines a similar increment of H. H is about 0.6 in the presence of the sole hydration water and rises above 0.7 when the water percentage is equal or above 15 %.

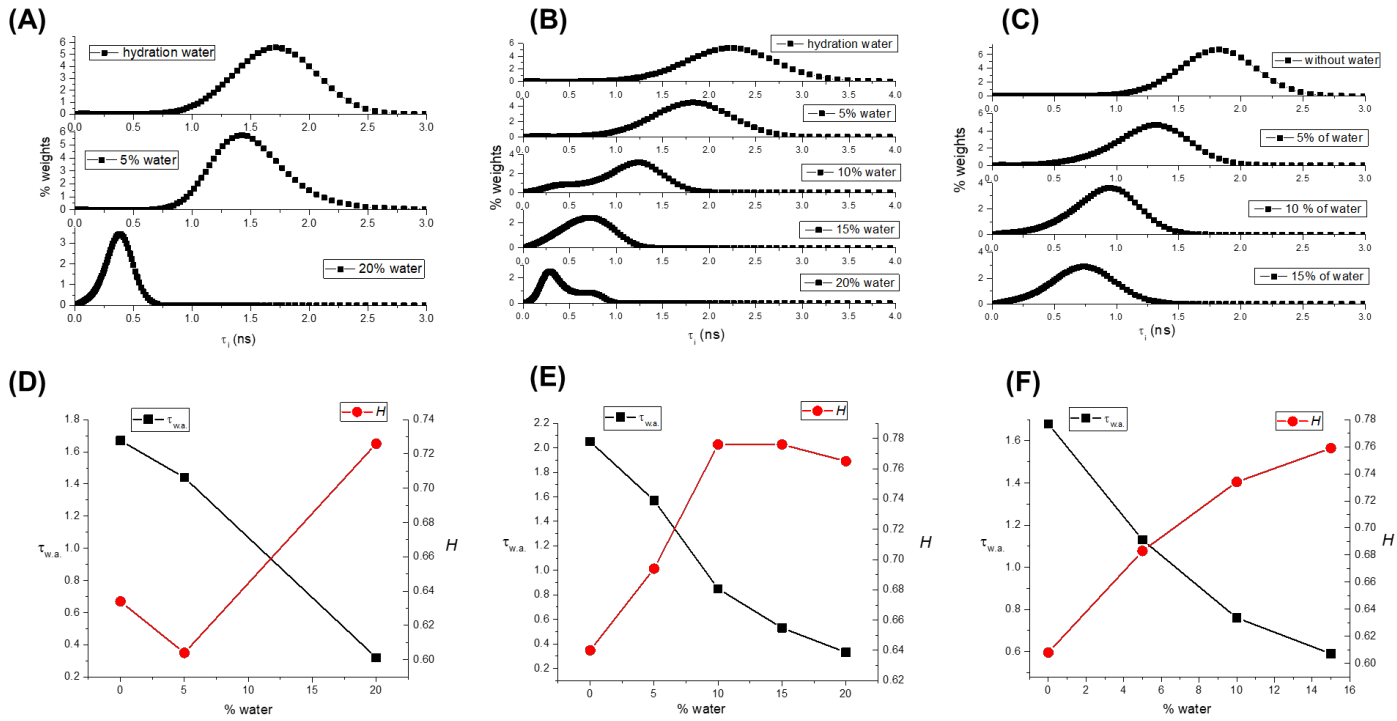

Figure 4. Lifetime distributions as functions of water content for PyI in **GLY/TMG** in (A), **pTSA/TBnAMSO** in (B), and **PhAA/DDDACl** in (C); trends of $\bar{\tau}_{w.a.}$ and *H* as functions of water % for PyI in **GLY/TMG** in (D), **pTSA/TBnAMSO** in (E), and **PhAA/DDDACl** in (F).

The second step of the studies on the water dilution was performed by time-resolved spectroscopy on the **GLY/TMG** hydrophilic system in the presence of increased water contents: femtosecond-resolved excited-sate absorption measurements were carried out on **PyI** dissolved in neat **GLY/TMG** and in the presence of 5%, 20% and 75% (w/w) of water (Figure 5 and S13). The obtained results are compared in Table 4 with the excited-state dynamics previously studied in a purely aqueous environment [51]. **PyI** dynamics in water is described by three transients, each exhibiting a specific spectral profile, whose main feature is a negative signal of stimulated emission red-shifting with time, as a consequence of excited-state relaxation. The dynamics is

extremely fast and the longest component, which is assigned to the relaxed TICT state, has a lifetime of less than 10 ps. On the other hand, when **PyI** is dissolved in **GLY/TMG** (Figure 5, left graph), its dynamics features much longer times and the $S_0 \leftarrow S_1$ transition happens in 1600 ps. However, not only gets slower the entire excited state dynamics, but also the transient assigned to a TICT state (with its stimulated emission peaking above 700 nm) is missing. This finding proves the impossibility for the fluorophore to undergo large amplitude motions in the DES and achieve a full relaxation. As the water content increases, the lifetime is reduced from 1600 ps to 400 ps and 240 ps with 5% and 20% of water respectively, reflecting the reduction of viscosity, but still no evidence of a fully relaxed TICT state emerges. This means that the DES is still able to impair **PyI** twisting, hence the HBD-HBA cluster formation among **GLY** and **TMG** couples is not prevented by such water additions. Only when the water content becomes prevalent, namely 75% w/w (Figure 5, right graph), a transient assignable to the TICT state, populated with a 4.2 ps dynamic and characterized by a lifetime of 18 ps and a stimulated emission band centred around 700 nm, is again detected. The difference in position and lifetime for this transient relatively to the same state observed in pure water could be due to some specific interactions between **PyI** and the single species forming the DES (Figure 5).

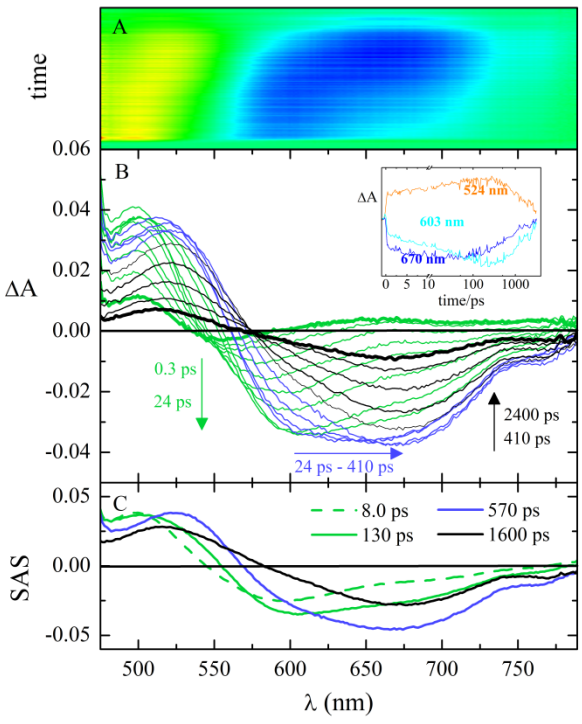

PyI in Gly/TMG

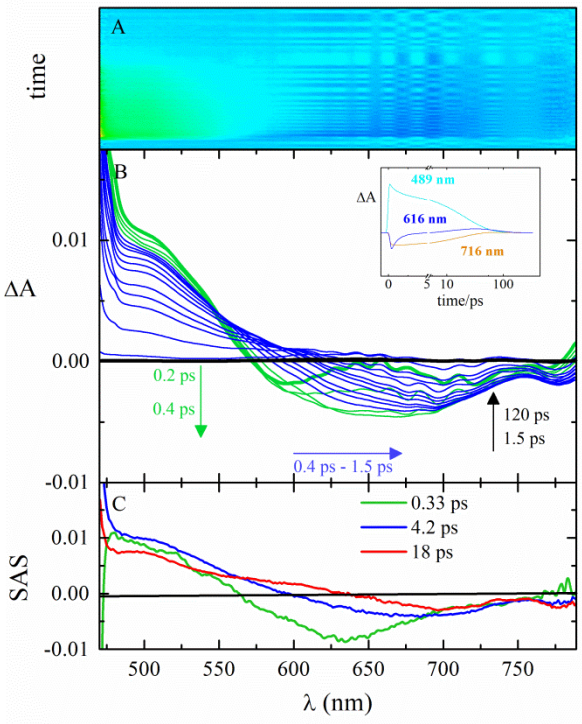

PyI in Gly/TMG +75%H_2O

Figure 5. Pump−probe absorption (λ_{exc}=400 nm) of **PyI** in neat **Gly/TMG** (left graph) and in **Gly/TMG** with 75% H_2O addition (right graph): A) contour plot of the experimental data, B) time resolved absorption spectra recorded at different delays after the laser pulse. Insets: decay kinetics recorded at meaningful wavelengths together with the corresponding fitting traces and C) Species Associated Spectra (SAS) of the decay components obtained by Target Analysis.

Table 4. Results of the Global Analysis of the femtosecond transient absorption experiments: exponential components revealed by the fitting with their spectral feature, i.e., maximum signal of stimulated emission (λ), and lifetime (τ). Data in water are reported for comparison purposes.

PyI in H_2O[a]		**PyI in Gly/TMG**							
				+5% H_2O		**+20% H_2O**		**+75% H_2O**	
λ (nm)	***τ (ps)***	***λ (nm)***	***τ (ps)***	***λ (nm)***	***τ (ps)***	***λ (nm)***	***τ (ps)***	***λ (nm)***	***τ (ps)***
580(–)	0.30	585(–)	8.0	595(–)	2.6	585(–)	1.0		
		600(–)	130	610(–)	19	610(–)	12	630(–)	0.33
		660(–)	570	660(–)	110	660(–)	68		
675(–)	0.70	675(–)	1600	675(–)	400	680(–)	240	685(–)	4.2
730(–)	8.6							700(–)	18

[a] From ref. [51]

As for the fastest transients describing the decay, they can be assigned to solvation processes, that is the relaxation of solvent molecules around the excited state of the solute. As a rule, solvation can be distinguished in ultrafast components due to small amplitude motions (librations and vibrations), known as inertial solvation, and slower components associated to larger motions (rotations and translations), known as diffusive solvation, which can also include hydrogen bond stretching when dealing with hydrogen-bonded systems [44,72] Common solvents are characterized by typical times for the solvation processes: in the case of water, the whole solvation relaxation happens within 1 ps, with inertial solvation being faster than 50 fs and diffusive solvation decaying in hundreds of femtoseconds [73,74].

Conversely, when **PyI** is dissolved in DESs, slow solvation decay times (up to hundreds of picoseconds) can be recognized, reflecting the enormous viscosity of the DESs, which impairs not only the aforementioned twisting of the solute, but also large molecular motions for the HBA and HBD couples forming the DES. In particular, the solvation of **PyI** in **Gly/TMG** is characterized by a complex dynamics described by three times of 8.0, 130, and 570 ps, respectively. When water is added to the systems in 5% and 20% w/w ratios, these solvation times get gradually shorter (Table 4), but a three-exponential dynamic is still observed. As previously seen for the TICT formation, it is only when water concentration rises to 75% that solvation resembles that of a common solvent,

revealing a single time of fractions of picoseconds (0.30 ps) assigned to diffusive solvation (other faster solvation dynamics might not be revealed because of the time resolution of our experimental setup). This evidence helps to obtain a clear picture of the **Gly/TMG** DES system under investigation: it features water-dependent viscosities, but maintains its microscopic structured order at least up to 20% (w/w) water additions [75].

Excited-state relaxation dynamics in DESs.

Finally, an excited-state absorption experiment was also performed on **PyI** dissolved into **U/ChCl** and **pTSA/TBnAMSO** DESs (Figure S14 and Table S3) in order to spot some differences between the various systems and shed some light on the unexpected behavior of the latter. **PyI** dynamic in **U/ChCl** and **pTSA/TBnAMSO** is again characterized by the absence of a transient assignable to the TICT state, which is thus not populated, as opposed to the presence of a three-exponential solvation dynamic, like the one observed in **Gly/TMG**. However, in the case of **U/ChCl**, these solvation processes occur with fairly reduced times (2.2, 31 and 230 ps). This finding corroborates the deduction made from the fluorescence study and MEM analysis about the greater viscosity experienced by the fluorescent probe **PyI** in **Gly/TMG** rather than in **U/ChCl**.

Interestingly enough, the solvation dynamics experienced by **PyI** in **pTSA/TBnAMSO** is instead described by somewhat shorter times relatively to **U/ChCl** as far as the first two solvation components are concerned (1.1 and 25 ps), but it exhibits a third component of 600 ps, markedly longer than the one recorded in **U/ChCl**, even slightly exceeding the longest solvation component in **Gly/TMG**. This slow component is confidently assigned to exchange diffusion processes in and out of the solvation shell and it is thus related to the long-range organization of the system. Hence, the evidence of a slowed-down diffusive solvation for the **pTSA/TBnAMSO** DES well agrees with the greatest bulk viscosity measured for it. Conversely, the shorter times revealed for the first solvation components, which are instead due to in-place molecular motions, can serve as an indication of a higher disorder in the cybotactic region of the probe. This might be explained by the chemical composition of the DES, inasmuch as **pTSA** molecules bring with them water molecules, whose presence around the solute can indeed be responsible for both the enhancement of local disorder (heterogeneity) and the reduction of local friction. All things considered, the excited state solvation dynamics of **PyI** in **pTSA/TBnAMSO** corroborates on the one hand the results of the fluorescence study and MEM analysis, which reveal a significant micro-

heterogeneity for this DES, and on the other hand, the appraisal of the greatest bulk viscosity among the investigated systems.

CONCLUSIONS

The two fluorescent probes have proved to be highly sensitive to the polarity, viscosity, hydrogen-bond network and micro-heterogeneity of various DESs, allowing even subtle differences between the investigated systems to be outlined.

Both probes, on the basis of their peculiar solvatochromic behaviors, enabled to classify the five DESs as a function of their polarity. The obtained results satisfactorily match between the two probes and a well-defined polarity ranking can thus be drawn: **PhAA/DDDACl > U/ChCl** $\simeq$ **GLY/TMG > pTSA/TBnAMSO > THY/DDDACl**. As for the viscosity of the DESs, in agreement with their bulk viscosity previously measured, both the fluorescence spectral profile and the Fuzzy Entropy values recorded for the **PyI** probe led to the following order from the most to the least viscous DES: **THY/DDDACl > GLY/TMG > U/ChCl**. However, **PhAA/DDDACl** and **pTSA/TBnAMSO** were found to exhibit distinctive features. The former, although characterized by the lowest bulk viscosity, impairs the excited state relaxation of **PyI** supposedly because of its preference to localize closely within the HBD-HBA pairs of the DES. Conversely, **pTSA/TBnAMSO** turned out to have the greatest bulk viscosity, but a reduced in-space viscosity around and close to the probe. These findings, deduced by the MEM results and the thorough analysis of the solvation dynamics detected in the excited state absorption experiment, imply, despite its marked long-range organization, a high local micro-heterogeneity for this system, supposedly related to the water molecule linked to the **pTSA** molecule.

As for the **X5** probe, owing to its fluorescence dependence on the proticity of the medium, it instead provided an insight into the hydrogen bond ability of the DESs, which was found to be the greatest for **DDDACl**-containing DESs.

Finally, the effect of water additions on either hydrophilic or hydrophobic DESs was investigated by fluorescence spectroscopy and MEM analysis of the **PyI** emission kinetics. As for the hydrophobic **PhAA/DDDACl** system, water additions were found to little affect the fluorescence properties of the probe and instead enhance its localization within the hydrophobic but highly polar domains made up of the HBD-HBA pairs. On the other hand, as is the case with hydrophilic DESs, pronounced water-dependent trends for the reduction of the viscosity and the

enhancement of the micro-heterogeneity were revealed in both **GLY/TMG** and **pTSA/TBnAMSO**. In the case of **GLY/TMG**, femtosecond-resolved transient absorption experiments corroborated the dependence of viscosity on the water content, and further, both the solvation dynamics of the DESs' molecules and the excited state relaxation of the **PyI** probe clarified that only at a 75% (w/w) water content **GLY/TMG** loses its microscopic structured order.

To sum up, this study provided interesting insights into the structural features, also at a molecular level, of various DESs. The multifaceted aspects of these novel solvents were indeed revealed, whose intimate understanding is of pivotal importance for the development of a plethora of new possible applications for these promising and fascinating media.

BIBLIOGRAPHY

[1] A. Paiva, R. Craveiro, I. Aroso, M. Martins, R.L. Reis, A.R.C. Duarte, Natural deep eutectic solvents–solvents for the 21st century, ACS Sustain. Chem. Eng. 2 (2014) 1063–1071.

[2] A. Shishov, A. Bulatov, M. Locatelli, S. Carradori, V. Andruch, Application of deep eutectic solvents in analytical chemistry. A review, Microchem. J. 135 (2017) 33–38.

[3] E.L. Smith, A.P. Abbott, K.S. Ryder, Deep eutectic solvents (DESs) and their applications, Chem. Rev. 114 (2014) 11060–11082.

[4] D.A. Alonso, A. Baeza, R. Chinchilla, G. Guillena, I.M. Pastor, D.J. Ramón, Deep eutectic solvents: The organic reaction medium of the century, European J. Org. Chem. 2016 (2016) 612–632.

[5] M.A.R. Martins, S.P. Pinho, J.A.P. Coutinho, Insights into the nature of eutectic and deep eutectic mixtures, J. Solution Chem. 48 (2019) 962–982.

[6] C.F. Araujo, J.A.P. Coutinho, M.M. Nolasco, S.F. Parker, P.J.A. Ribeiro-Claro, S. Rudić, B.I.G. Soares, P.D. Vaz, Inelastic neutron scattering study of reline: shedding light on the hydrogen bonding network of deep eutectic solvents, Phys. Chem. Chem. Phys. 19 (2017) 17998–18009.

[7] N. Schaeffer, J.H.F. Conceição, M.A.R. Martins, M.C. Neves, G. Pérez-Sánchez, J.R.B. Gomes, N. Papaiconomou, J.A.P. Coutinho, Non-ionic hydrophobic eutectics–versatile solvents for tailored metal separation and valorisation, Green Chem. 22 (2020) 2810–2820.

[8] R. Germani, M. Orlandini, M. Tiecco, T. Del Giacco, Novel low viscous, green and amphiphilic N-oxides/phenylacetic acid based Deep Eutectic Solvents, J. Mol. Liq. 240 (2017) 233–239.

doi:10.1016/j.molliq.2017.05.084.

[9] J. Torregrosa-Crespo, X. Marset, G. Guillena, D.J. Ramón, R.M. Martínez-Espinosa, New guidelines for testing “Deep eutectic solvents” toxicity and their effects on the environment and living beings, Sci. Total Environ. 704 (2020) 135382.

[10] M. Ballarotto, F. Cappellini, R. Maestri, T. Del Giacco, P. Di Profio, M. Tiecco, R. Germani, Exploring the acidic catalytic role of differently structured deep eutectic solvents in the aza-Michael addition of amines to 2-vinylpiridine, Monatshefte F¸r Chemie. (2020). doi:10.1007/s00706-020-02660-z.

[11] Y.H. Choi, J. van Spronsen, Y. Dai, M. Verberne, F. Hollmann, I.W.C.E. Arends, G.-J. Witkamp, R. Verpoorte, Are natural deep eutectic solvents the missing link in understanding cellular metabolism and physiology?, Plant Physiol. 156 (2011) 1701–1705.

[12] F. Cardellini, M. Tiecco, R. Germani, G. Cardinali, L. Corte, L. Roscini, N. Spreti, Novel zwitterionic deep eutectic solvents from trimethylglycine and carboxylic acids: Characterization of their properties and their toxicity, RSC Adv. 4 (2014) 55990–56002. doi:10.1039/C4RA10628H.

[13] K. Shahbaz, F.S. Mjalli, G. Vakili-Nezhaad, I.M. AlNashef, A. Asadov, M.M. Farid, Thermogravimetric measurement of deep eutectic solvents vapor pressure, J. Mol. Liq. 222 (2016) 61–66.

[14] I. Juneidi, M. Hayyan, M.A. Hashim, Evaluation of toxicity and biodegradability for cholinium-based deep eutectic solvents, RSC Adv. 5 (2015) 83636–83647.

[15] M. Hayyan, M.A. Hashim, A. Hayyan, M.A. Al-Saadi, I.M. AlNashef, M.E.S. Mirghani, O.K. Saheed, Are deep eutectic solvents benign or toxic?, Chemosphere. 90 (2013) 2193–2195.

[16] K. Radošević, M.C. Bubalo, V.G. Srček, D. Grgas, T.L. Dragičević, I.R. Redovniković, Evaluation of toxicity and biodegradability of choline chloride based deep eutectic solvents, Ecotoxicol. Environ. Saf. 112 (2015) 46–53.

[17] Y. Dai, J. van Spronsen, G.-J. Witkamp, R. Verpoorte, Y.H. Choi, Natural deep eutectic solvents as new potential media for green technology, Anal. Chim. Acta. 766 (2013) 61–68.

[18] Q. Wen, J.-X. Chen, Y.-L. Tang, J. Wang, Z. Yang, Assessing the toxicity and biodegradability of deep eutectic solvents, Chemosphere. 132 (2015) 63–69.

[19] E. Durand, J. Lecomte, P. Villeneuve, From green chemistry to nature: the versatile role of low transition temperature mixtures, Biochimie. 120 (2016) 119–123.

[20] C. Florindo, F. Lima, B.D. Ribeiro, I.M. Marrucho, Deep eutectic solvents: overcoming 21st

century challenges, Curr. Opin. Green Sustain. Chem. 18 (2019) 31–36.

[21] A. Fontana, R. Zappacosta, R. Germani, S. Boncompagni, A. Di Crescenzo, G. Siani, P. Di Profio, V. Ettorre, M. Tiecco, Novel zwitterionic Natural Deep Eutectic Solvents as environmentally friendly media for spontaneous self-assembly of gold nanoparticles, J. Mol. Liq. 268 (2018) 371–375. doi:10.1016/j.molliq.2018.07.060.

[22] F. Curti, G. Abbiati, V. Pirovano, A. Caselli, R. Germani, M. Tiecco, E. Rossi, p-TSA-Based DESs as "Active Green Solvents" for Microwave Enhanced Cyclization of 2-Alkynyl-(hetero)-arylcarboxylates: an Alternative Access to 6-Substituted 3,4-Fused 2-Pyranones, European J. Org. Chem. (2019). doi:10.1002/ejoc.201801884.

[23] P. Liu, J.-W. Hao, L.-P. Mo, Z.-H. Zhang, Recent advances in the application of deep eutectic solvents as sustainable media as well as catalysts in organic reactions, RSC Adv. 5 (2015) 48675–48704.

[24] H. Qin, X. Hu, J. Wang, H. Cheng, L. Chen, Z. Qi, Overview of acidic deep eutectic solvents on synthesis, properties and applications, Green Energy Environ. 5 (2020) 8–21.

[25] F. Liu, Z. Xue, X. Zhao, H. Mou, J. He, T. Mu, Catalytic deep eutectic solvents for highly efficient conversion of cellulose to gluconic acid with gluconic acid self-precipitation separation, Chem. Commun. 54 (2018) 6140–6143.

[26] T. Palomba, G. Ciancaleoni, T. Del Giacco, R. Germani, F. Ianni, M. Tiecco, Deep Eutectic Solvents formed by chiral components as chiral reaction media and studies of their structural properties, J. Mol. Liq. 262 (2018) 285–294. doi:10.1016/j.molliq.2018.04.096.

[27] M. Tiecco, D.A. Alonso, D.R. Ñíguez, G. Ciancaleoni, G. Guillena, D.J. Ramón, A.A. Bonillo, R. Germani, Assessment of the organocatalytic activity of chiral L-Proline-based Deep Eutectic Solvents based on their structural features, J. Mol. Liq. 313 (2020) 113573. doi:10.1016/j.molliq.2020.113573.

[28] S. Nejrotti, M. Iannicelli, S.S. Jamil, D. Arnodo, M. Blangetti, C. Prandi, Natural deep eutectic solvents as an efficient and reusable active system for the Nazarov cyclization, Green Chem. 22 (2020) 110–117.

[29] S.K. Shukla, D. Nikjoo, J.-P. Mikkola, Is basicity the sole criterion for attaining high carbon dioxide capture in deep-eutectic solvents?, Phys. Chem. Chem. Phys. 22 (2020) 966–970.

[30] G. Carrasco-Huertas, R.J. Jiménez-Riobóo, M.C. Gutiérrez, M.L. Ferrer, F. del Monte, Carbon and carbon composites obtained using deep eutectic solvents and aqueous dilutions thereof, Chem. Commun. 56 (2020) 3592–3604.

[31] F. Gabriele, M. Chiarini, R. Germani, M. Tiecco, N. Spreti, Effect of water addition on choline chloride/glycol deep eutectic solvents: Characterization of their structural and physicochemical properties, J. Mol. Liq. 291 (2019) 111301. doi:10.1016/j.molliq.2019.111301.

[32] C. Ma, A. Laaksonen, C. Liu, X. Lu, X. Ji, The peculiar effect of water on ionic liquids and deep eutectic solvents, Chem. Soc. Rev. (2018).

[33] F.O. Farias, H. Passos, M.G. Sanglard, L. Igarashi-Mafra, J.A.P. Coutinho, M.R. Mafra, Designer solvent ability of alcohols in aqueous biphasic systems composed of deep eutectic solvents and potassium phosphate, Sep. Purif. Technol. 200 (2018) 84–93.

[34] M. Tiecco, F. Cappellini, F. Nicoletti, T. Del Giacco, R. Germani, P. Di Profio, Role of the hydrogen bond donor component for a proper development of novel hydrophobic deep eutectic solvents, J. Mol. Liq. 281 (2019) 423–430. doi:10.1016/j.molliq.2019.02.107.

[35] D.J.G.P. van Osch, L.F. Zubeir, A. van den Bruinhorst, M.A.A. Rocha, M.C. Kroon, Hydrophobic deep eutectic solvents as water-immiscible extractants, Green Chem. 17 (2015) 4518–4521. doi:10.1039/C5GC01451D.

[36] S. Kaur, A. Malik, H.K. Kashyap, Anatomy of microscopic structure of ethaline deep eutectic solvent decoded through molecular dynamics simulations, J. Phys. Chem. B. 123 (2019) 8291–8299.

[37] S. Kaur, A. Gupta, H.K. Kashyap, Nanoscale spatial heterogeneity in deep eutectic solvents, J. Phys. Chem. B. 120 (2016) 6712–6720.

[38] X.-D. Hou, A.-L. Li, K.-P. Lin, Y.-Y. Wang, Z.-Y. Kuang, S.-L. Cao, Insight into the structure-function relationships of deep eutectic solvents during rice straw pretreatment, Bioresour. Technol. 249 (2018) 261–267.

[39] L. Brinchi, R. Germani, E. Braccalenti, N. Spreti, M. Tiecco, G. Savelli, Accelerated decarboxylation of 6-nitrobenzisoxazole-3-carboxylate in imidazolium-based ionic liquids and surfactant ionic liquids, J. Colloid Interface Sci. 348 (2010) 137–145. doi:10.1016/j.jcis.2010.04.029.

[40] D. Dhingra, Bhawna, A. Pandey, S. Pandey, Pyrene Fluorescence To Probe a Lithium Chloride-Added (Choline Chloride+ Urea) Deep Eutectic Solvent, J. Phys. Chem. B. 123 (2019) 3103–3111.

[41] S.S. Hossain, A. Samanta, Solute rotation and translation dynamics in an ionic deep eutectic solvent based on choline chloride, J. Phys. Chem. B. 121 (2017) 10556–10565.

[42] N. Subba, E. Tarif, P. Sen, R. Biswas, Subpicosecond Solvation Response and Partial Viscosity Decoupling of Solute Diffusion in Ionic Acetamide Deep Eutectic Solvents: Fluorescence Up-Conversion and Fluorescence Correlation Spectroscopic Measurements, J. Phys. Chem. B. 124 (2020) 1995–2005.

[43] E. Tarif, J. Mondal, R. Biswas, Interaction and dynamics in a fully biodegradable glucose-containing naturally abundant deep eutectic solvent: temperature-dependent time-resolved fluorescence measurements, J. Phys. Chem. B. 123 (2019) 9378–9387.

[44] N. Subba, K. Polok, P. Piatkowski, B. Ratajska-Gadomska, R. Biswas, W. Gadomski, P. Sen, Temperature-Dependent Ultrafast Solvation Response and Solute Diffusion in Acetamide–Urea Deep Eutectic Solvent, J. Phys. Chem. B. 123 (2019) 9212–9221.

[45] A.H. Turner, D. Kim, Rotation and translation dynamics of coumarin 153 in choline chloride-based deep eutectic solvents, J. Chem. Phys. 149 (2018) 174503.

[46] S. Chatterjee, D. Ghosh, T. Haldar, P. Deb, S.S. Sakpal, S.H. Deshmukh, S.M. Kashid, S. Bagchi, Hydrocarbon Chain-Length Dependence of Solvation Dynamics in Alcohol-Based Deep Eutectic Solvents: A Two-Dimensional Infrared Spectroscopic Investigation, J. Phys. Chem. B. 123 (2019) 9355–9363.

[47] S. Chatterjee, T. Haldar, D. Ghosh, S. Bagchi, Electrostatic Manifestation of Micro-Heterogeneous Solvation Structures in Deep-Eutectic Solvents: A Spectroscopic Approach, J. Phys. Chem. B. 124 (2020) 3709–3715.

[48] S.S. Hossain, S. Paul, A. Samanta, Complete Solvation Dynamics of Coumarin 153 in Tetraalkylammonium Bromide-Based Deep Eutectic Solvents, J. Phys. Chem. B. 124 (2020) 2473–2481.

[49] Y. Cui, K.D. Fulfer, J. Ma, T.K. Weldeghiorghis, D.G. Kuroda, Solvation dynamics of an ionic probe in choline chloride-based deep eutectic solvents, Phys. Chem. Chem. Phys. 18 (2016) 31471–31479.

[50] C. Bonaccorso, A. Cesaretti, F. Elisei, L. Mencaroni, A. Spalletti, C.G. Fortuna, New Styryl Phenanthroline Derivatives as Model D− π− A− π− D Materials for Non-Linear Optics, ChemPhysChem. 19 (2018) 1917–1929.

[51] B. Carlotti, A. Cesaretti, C.G. Fortuna, A. Spalletti, F. Elisei, Experimental evidence of dual emission in a negatively solvatochromic push–pull pyridinium derivative, Phys. Chem. Chem. Phys. 17 (2015) 1877–1882.

[52] A. Cesaretti, C. Bonaccorso, V. Carboni, M.S. Giubila, C.G. Fortuna, F. Elisei, A. Spalletti, Four

styryl phenanthroline derivatives as excellent acidochromic probes, Dye. Pigment. 162 (2019) 440–450.

[53] A. Cesaretti, I. Di Guida, N.E. Caldero-Rodríguez, C. Clementi, R. Germani, P.L. Gentili, Mimicking the Secretory Action of a Gland by a Composite System Made of a pH-Responsive Surfactant-Based Hydrogel and a Dialysis Membrane, ACS Omega. 3 (2018) 16777–16783.

[54] A. Cesaretti, P. Foggi, C.G. Fortuna, F. Elisei, A. Spalletti, B. Carlotti, Uncovering Structure–Property Relationships in Push–Pull Chromophores: A Promising Route to Large Hyperpolarizability and Two-Photon Absorption, J. Phys. Chem. C. 124 (2020) 15739–15748.

[55] V. De Santi, F. Cardellini, L. Brinchi, R. Germani, Novel Brønsted acidic deep eutectic solvent as reaction media for esterification of carboxylic acid with alcohols, Tetrahedron Lett. 53 (2012) 5151–5155.

[56] C. Burgdorff, S. Ehrhardt, H.G. Loehmannsroeben, Photophysical properties of tetracene derivatives in solution. 2. Halogenated tetracene derivatives, J. Phys. Chem. 95 (1991) 4246–4249.

[57] P.J. Steinbach, R. Ionescu, C.R. Matthews, Analysis of kinetics using a hybrid maximum-entropy/nonlinear-least-squares method: application to protein folding, Biophys. J. 82 (2002) 2244–2255.

[58] P.J. Steinbach, Inferring lifetime distributions from kinetics by maximizing entropy using a bootstrapped model, J. Chem. Inf. Comput. Sci. 42 (2002) 1476–1478.

[59] B. Carlotti, A. Cesaretti, P.L. Gentili, A. Marrocchi, F. Elisei, A. Spalletti, A two excited state model to explain the peculiar photobehaviour of a flexible quadrupolar D–π–D anthracene derivative, Phys. Chem. Chem. Phys. 18 (2016) 23389–23399.

[60] A. Cesaretti, B. Carlotti, G. Consiglio, T. Del Giacco, A. Spalletti, F. Elisei, Inclusion of two push–pull N-methylpyridinium salts in anionic surfactant solutions: A comprehensive photophysical investigation, J. Phys. Chem. B. 119 (2015) 6658–6667.

[61] A. Cesaretti, B. Carlotti, C. Clementi, R. Germani, F. Elisei, Effect of micellar and sol–gel media on the spectral and kinetic properties of tetracycline and its complexes with Mg 2+, Photochem. Photobiol. Sci. 13 (2014) 509–520.

[62] J. Snellenburg, S. Laptenok, R. Seger, K. Mullen, I. Van Stokkum, Glotaran: A Java-based graphical user interface for the R package TIMP, (2012).

[63] A. Cesaretti, B. Carlotti, R. Germani, A. Spalletti, F. Elisei, Inclusion of push–pull N-methylpyridinium salts within surfactant hydrogels: is their excited state intramolecular

charge transfer mediated by twisting?, Phys. Chem. Chem. Phys. 17 (2015) 17214–17220.

[64] M. Gambucci, P.L. Gentili, P. Sassi, L. Latterini, A multi-spectroscopic approach to investigate the interactions between Gramicidin A and silver nanoparticles, Soft Matter. 15 (2019) 6571–6580.

[65] G. Massaro, P.L. Gentili, V. Ambrogi, M. Nocchetti, F. Marmottini, F. Ortica, L. Latterini, Triplet-triplet annihilation based upconversion in silica matrices, Microporous Mesoporous Mater. 246 (2017) 120–129.

[66] P.L. Gentili, The fuzziness of a chromogenic spirooxazine, Dye. Pigment. 110 (2014) 235–248.

[67] P.L. Gentili, The fuzziness of the molecular world and its perspectives, Molecules. 23 (2018) 2074.

[68] P.L. Gentili, C. Clementi, A. Romani, Ultraviolet–visible absorption and luminescence properties of quinacridone–barium sulfate solid mixtures, Appl. Spectrosc. 64 (2010) 923–929.

[69] A. Cesaretti, B. Carlotti, P.L. Gentili, C. Clementi, R. Germani, F. Elisei, Doxycycline and oxytetracycline loading of a zwitterionic amphoteric surfactant-gel and their controlled release, Phys. Chem. Chem. Phys. 16 (2014) 23096–23107.

[70] A. Cesaretti, B. Carlotti, P.L. Gentili, R. Germani, A. Spalletti, F. Elisei, Twisting in the excited state of an N-methylpyridinium fluorescent dye modulated by nano-heterogeneous micellar systems, Photochem. Photobiol. Sci. 15 (2016) 525–535.

[71] Y. Dai, G.-J. Witkamp, R. Verpoorte, Y.H. Choi, Tailoring properties of natural deep eutectic solvents with water to facilitate their applications, Food Chem. 187 (2015) 14–19.

[72] M.L. Horng, J.A. Gardecki, A. Papazyan, M. Maroncelli, Subpicosecond measurements of polar solvation dynamics: coumarin 153 revisited, J. Phys. Chem. 99 (1995) 17311–17337.

[73] S. Roy, B. Bagchi, Solvation dynamics in liquid water. A novel interplay between librational and diffusive modes, J. Chem. Phys. 99 (1993) 9938–9943.

[74] R. Jimenez, G.R. Fleming, P. V Kumar, M. Maroncelli, Femtosecond solvation dynamics of water, Nature. 369 (1994) 471–473.

[75] O.S. Hammond, D.T. Bowron, K.J. Edler, The effect of water upon deep eutectic solvent nanostructure: An unusual transition from ionic mixture to aqueous solution, Angew. Chemie Int. Ed. 56 (2017) 9782–9785.